SIAM J. APPL. MATH.
Vol. 73, No. 6, pp. 1959–1979

NONLINEAR WAVE PACKETS IN DEFORMED HONEYCOMB LATTICES*

MARK J. ABLOWITZ† AND YI ZHU‡

Abstract. The spectrum of a Schrödinger operator with a perfect honeycomb lattice potential has special points, called Dirac points, where the lowest two branches of the spectrum touch. Deformations can result in the merging and disappearance of the Dirac points, and the originally intersecting dispersion relation branches separate. Corresponding to these deformations, nonlinear envelope equations are derived and their dynamics are studied. In the region where Dirac points exist, a maximally balanced equation is derived which has limits to a nonlinear Schrödinger–Kadomtsev–Petviashvili (NLSKP)-type equation and its dispersionless reduction. When the Dirac points disappear and a gap opens, a different maximally balanced equation is derived which has the NLSKP equation and a one-dimensional nonlocal evolution equation as limits. When the gap is sufficiently wide, a nonlinear Dirac equation with nonzero mass and a nonlinear Schrödinger focusing-defocusing system are found. The latter two equations admit nonlinear localized modes. Typical dynamical behaviors of the effective envelope equations are presented.

Key words. honeycomb lattice, long wave approximation, effective dynamics, nonlinear Schrödinger equation, Kadomtsev–Petviashvili equation

AMS subject classifications. 41A60, 35C20, 35Q55, 35L60

DOI. 10.1137/120887618

1. Introduction.

Wave dynamics with a background two-dimensional honeycomb lattice is an area of research which has generated considerable interest; this is partly due to the fact that it arises in many applications. For example, the underlying atomic structure of graphene has a hexagonal honeycomb periodic structure [25, 24]. Other interesting applications where honeycomb lattices play an important role include Bose–Einstein condensation (BEC) associated with the dynamics of condensates in honeycomb optical lattices [35, 16], nonlinear optical beam propagation in photonic honeycomb crystals [26, 9], broken time-reversal symmetry [17], and propagation of nonlinear optical waves with a shallow honeycomb lattice background [6].

A special feature of honeycomb lattices is that the lowest band of the dispersion relation associated with the Schrödinger operator has two intersecting branches with isolated intersection points which are called Dirac points. In the vicinity of these Dirac points, the dispersion relation is conical. Many interesting physical phenomena are related to the existence of Dirac points such as conical diffraction, anomalous quantum Hall effects, Klein tunneling, and enhanced conductivity [25, 24, 35, 26]. These phenomena are related to the linear Dirac dynamics. Recently, a detailed mathematical study detailing the existence of Dirac points associated with the Schrödinger operator with a periodic potential has been developed [13, 14].

*Received by the editors August 9, 2012; accepted for publication (in revised form) July 31, 2013; published electronically November 7, 2013. This research was partially supported by the NFSC under grant 11204155, by the U.S. Air Force Office of Scientific Research under grant FA9550-12-1-0207, by the NSF under grants DMS-0905779 and CHE 1125935, and by the Tsinghua University Initiative Scientific Research Program.

http://www.siam.org/journals/siap/73-6/88761.html

†Department of Applied Mathematics, University of Colorado, 526 UCB, Boulder, CO 80309-0526 (mark.ablowitz@colorado.edu).

‡Corresponding author. Zhou Pei-Yuan Center for Applied Mathematics, Tsinghua University, Beijing 100084, China (yizhu@tsinghua.edu.cn).

Due to the important physical applications in optics and BEC literatures, nonlinear wave packets near the Dirac points have recently been considered [26, 9], and reduced equations have been derived which describe conical and triangular diffraction [10, 4]. Away from Dirac points the wave dynamics changes considerably, and nonlinear Schrödinger (NLS)-type equations govern the dynamics [4]. To study nonlinear wave packets in problems with background periodic structure one frequently constructs associated Bloch waves and then studies their nonlinear interactions. Direct calculations are usually complicated and require detailed numerical calculations. Alternatively, discrete approximations can sometimes be employed in the strong potential or tight-binding regime where this approximation is asymptotically accurate and the Bloch modes as well as their nonlinear interactions can be constructed analytically.

In some problems, the honeycomb lattice is deformed [8]. This results in the so-called "nearest neighbor hopping energies" not being equal; i.e., $\rho \neq \rho_0 = 1$ (see Figure 1). If the honeycomb lattice is made up of perfect hexagons, all nearest neighbor hopping energies are equal; i.e., $\rho = \rho_0 = 1$. Deformed lattices correspond to $\rho \neq 1$; ρ, or more conveniently $\beta = 2\rho - 1$, plays the role of the deformation parameter. As a consequence of the deformation the Dirac points may disappear and a gap may develop between the two lowest bands. Physically, band touching and band separation give rise to different physical properties and different associated dynamics. Here we employ long wave approximation which corresponds to the regime where the envelope scale is much larger than the lattice scale. From a mathematical point of view, the dynamics in this limit corresponds to the slowly varying wave approximation. This is a particularly interesting topic in both physics and applied mathematics. To date, the envelope dynamics associated with nondegenerate points on the dispersion surfaces has been investigated in detail; cf. [15, 7, 31]. Similarly, wave envelopes associated with gap solitons and their properties have also been widely investigated; cf. [21, 12, 30, 18]. However, there are few results known related to the dynamics associated with singular points such as Dirac points in the dispersion surfaces. This conical crossing results in the nonsmoothness of the dispersion relation and mathematical difficulties when using a direct multiscale expansion or WKB method.

This work focuses on finding the leading order reduced asymptotic equations corresponding to the deformation of the lattice as the locations of the Dirac points are modified, merge, and a gap appears. We trace the equations and dynamics from conical to elliptical to "straight-line" diffraction, all the way through to the development of the localization of modes. Interestingly we find certain novel maximal balanced leading order equations governing this situation. Two of the reduced effective equations we term NLSKP and NLSKZ, as they are NLS analogues of the Kadomstsev–Petviashvili (KP) equation [19, 1] and its dispersionless reduction [22, 34].

The organization of this work is as follows. In sections 2 and 3, we discuss and outline some basic information about honeycomb lattices, suitable orbital approximations, and the corresponding linear spectrum. In section 4, the long wave approximation of the discrete equation is formulated; this will be used to find the continuous envelope equations associated with the special points in the Brillouin zone. In sections 5 and 6, we derive the associated reduced asymptotic equations, via multiple scale perturbation analysis, in different regimes. In particular in section 5 we investigate the situation when Dirac points exist. When there is little deformation, then a standard nonlinear Dirac system applies, and conical/elliptical/triangular diffraction results. When we are close to merging ($0 < 2\rho - 1 = \beta \ll 1$), we find a key maximally balanced (nonlocal) equation, (5.4), which in turn has limiting forms to what we refer

as NLSKZ and NLSKP equations. In section 6 we investigate the case when a gap in the spectrum is present ($\beta < 0$). When there is a sufficiently small gap, then again there is a central maximally balanced (nonlocal) equation, (6.2), which has limiting forms to an NLSKP equation and a 1+1 (one "space" variable and one evolution variable)-dimensional nonlocal equation, (6.4). As the gap becomes larger, but still small, we find a nonlinear Dirac equation with nonzero mass, (6.5). Finally, when the gap width is no longer asymptotically small, we find a coupled focusing-defocusing NLS system, (6.6). The latter two equations have localized (soliton) solutions. In section 7, we give a brief summary of the limiting envelope dynamics and some remarks on the corresponding numerical simulations. In section 8, we conclude and discuss the main results.

2. Honeycomb lattices and discrete coupled mode equations. Consider the following normalized two-dimensional lattice NLS equation:

$$i\partial_z\psi + \Delta\psi - V(\mathbf{r})\psi + \sigma|\psi|^2\psi = 0, \tag{2.1}$$

where Δ is the two-dimensional Laplacian, $V(\mathbf{r})$ is a honeycomb lattice; i.e., $V(\mathbf{r}+\mathbf{v}) = V(\mathbf{r})$ $\forall \mathbf{v} \in \Gamma$, and its local minima are located at $\Gamma_{\mathbf{H}}$, where Γ and $\Gamma_{\mathbf{H}}$ are defined later. Lattice NLS equations are frequently used to describe light propagation in photonic crystals [32, 33] and the dynamics of Bose–Einstein condensates trapped in optic lattices [23]. In the latter field, this equation is usually referred to as the Gross–Pitaevskii equation [27]. Due to its special features and many applications, the lattice NLS equation in the presence of honeycomb lattices is an interesting system to study; to date, most research has focused on either the strong or the weak potential limits, because the dispersion relation, Bloch waves, and their nonlinear interactions can be analytically constructed under these two limits. Recently Fefferman and Weinstein developed a rigorous theory of Dirac points [13] and associated linear dynamics [14] beyond these two limiting cases. Their results pave the way for obtaining additional rigorous mathematical results in the generic regime near Dirac points. Unfortunately, developing higher order dispersion structure and nonlinear interactions of Bloch waves is still not straightforward. Furthermore the limiting cases provide considerable physical insight. In the literature, the discrete approximation in the tight-binding limit is often used. In this paper, we begin our analysis from a discrete coupled mode system, (2.4), which is derived from the tight-binding approximation to the above lattice NLS equation (2.1); cf. [4].

Let $\Gamma \simeq \mathbb{Z}^2$ denote a two-dimensional lattice generated through the basis $\{\mathbf{v}_1, \mathbf{v}_2\}$, i.e.,

$$\Gamma = \{m\mathbf{v}_1 + n\mathbf{v}_2 : \quad m, n \in \mathbb{Z}\}.$$

The primitive unit cell Ω is defined as

$$\Omega = \{q_1\mathbf{v}_1 + q_2\mathbf{v}_2 : q_j \in [0, 1)\}.$$

The primitive cell Ω is the fundamental tile of a tessellation of the plane associated with the lattice Γ, i.e., $\mathbb{R}^2 = \bigcup_{\mathbf{v}\in\Gamma}(\Omega + \mathbf{v})$.

Consider a special two-dimensional triangular lattice, whose basis vectors satisfy $\mathbf{v}_2 = R\mathbf{v}_1$, where the rotation matrix R rotates a vector in $\mathbb{R}^2$ clockwise by $\pi/3$. R is given by

$$R = \begin{pmatrix} \frac{1}{2} & \frac{\sqrt{3}}{2} \\ -\frac{\sqrt{3}}{2} & \frac{1}{2} \end{pmatrix}.$$

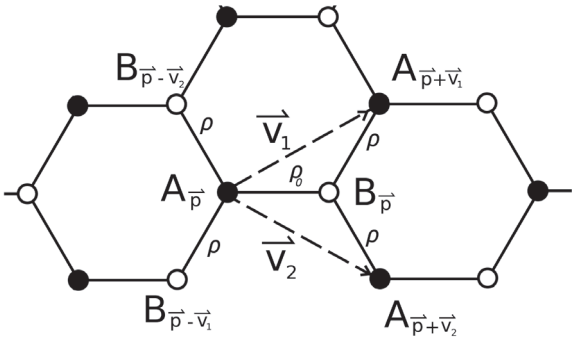

FIG. 1. *A honeycomb lattice is composed of two triangular sublattices,* $\Gamma_{\mathbf{A}}$ *(dots) and* $\Gamma_{\mathbf{B}}$ *(circles), generated by* $\mathbf{v}_1$ *and* $\mathbf{v}_2$ *from different beginning points. Here* ρ *and* ρ_0 *are nearest neighbor hopping energies in the tight-binding limit. In this work,* $\rho_0 = 1$.

A honeycomb lattice is composed of two triangular sublattices. Namely, there are two initial points $\mathbf{A} \in \Omega$ and $\mathbf{B} \in \Omega$, where $\mathbf{A} \neq \mathbf{B}$; then the two sublattices are

$$\Gamma_{\mathbf{A}} = \mathbf{A} + \Gamma, \qquad \Gamma_{\mathbf{B}} = \mathbf{B} + \Gamma.$$

A honeycomb lattice is the union of the two sublattices, i.e.,

$$\Gamma_{\mathbf{H}} = \Gamma_{\mathbf{A}} \cup \Gamma_{\mathbf{B}}.$$

It is noted that a honeycomb lattice and the corresponding triangle lattice have the same unit cell Ω which is equivalent to a hexagon due to the periodicity. However, a honeycomb potential has two minima in a cell, while the triangle potential has only one. These minima of a potential are usually referred to as the locations where atoms, nuclei, or the maximal refractive index are located. The corresponding Bloch waves are very different between these two lattices.

A honeycomb lattice and corresponding indices used herein are displayed in Figure 1. All dots are $\mathbf{A}$ lattice points, and all circles are $\mathbf{B}$ lattice points. We see that an $\mathbf{A}$ lattice point $\mathbf{A_p} \in \Gamma_{\mathbf{A}}$ has three nearest neighbors that are all $\mathbf{B}$ lattice points: $\mathbf{B_p}$, $\mathbf{B_{p-v_1}}$, and $\mathbf{B_{p-v_2}}$; a $\mathbf{B}$ lattice point has three nearest neighbors that are all $\mathbf{A}$ lattice points: $\mathbf{A_p}$, $\mathbf{A_{p+v_1}}$, and $\mathbf{A_{p+v_2}}$.

The dual lattice Γ' is spanned by the dual basis vectors $\mathbf{k}_1$ and $\mathbf{k}_2$, where $\mathbf{k}_m \cdot \mathbf{v}_n = 2\pi\delta_{mn}$; i.e., $\Gamma' = \{m\mathbf{k}_1 + n\mathbf{k}_2 : \ m, n \in \mathbb{Z}\}$. The primitive dual unit cell Ω' is defined as

$$\Omega' = \left\{ q_1\mathbf{k}_1 + q_2\mathbf{k}_2 : q_j \in \left[-\frac{1}{2}, \frac{1}{2} \right) \right\}.$$

This is also called the Brillouin zone.

The nonlinear evolution depends on the properties of the associated linear eigenvalue problem, namely,

$$(-\Delta + V(\mathbf{r}))\varphi_n = \mu_n \varphi_n, \tag{2.2}$$

where φ is called a Bloch mode and $n = 1, 2, \ldots$ denotes the band index. From the Bloch–Floquet theorem, $\varphi_n = e^{i\mathbf{kr}} U_n(\mathbf{r}; \mathbf{k})$, where $U_n(\mathbf{r} + \mathbf{v}; \cdot) = U_n(\mathbf{r}; \cdot)$ $\forall \mathbf{v} \in$

Γ. The dispersion relation $\mu_n(\mathbf{k})$ is defined in the Brillouin zone Ω'. Alternatively, $\mu_n(\mathbf{k}+\mathbf{k}') = \mu_n(\mathbf{k}) \forall \mathbf{k}' \in \Gamma'$. Similar to the Fourier decomposition, $\{\varphi_n(\mathbf{r};\mathbf{k})\}_{n\in\mathbb{N},\mathbf{k}\in\Omega'}$ is a complete set in $L^2(\mathbb{R}^2)$ [29].

The analytical structure of the dispersion relation $\mu_n(\mathbf{k})$ and associated Bloch modes in two dimensions are, in general, quite complex. In the tight-binding limit ($|V| \gg 1$), the Bloch modes are highly localized near the lattice minima. The main features of the Bloch modes are determined by the potential in the vicinity of the minima. Due to the underlying periodicity, one needs only to construct a one-well potential in the full plane, which coincides with the lattice potential in the vicinity of a typical minima. The associated eigenfunctions are often referred as the "orbitals." Then the Bloch modes are approximated by the linear combinations of the orbitals at different minima. A rigorous study on this approximation can be found in [2].

Suppose that $\phi_A(\mathbf{r})$ and $\phi_B(\mathbf{r})$ are the orbitals associated with the $\mathbf{A}$ and $\mathbf{B}$ lattices, respectively (see [4, 2] for details). $\{(\phi_A(\mathbf{r}-\mathbf{v}), \phi_B(\mathbf{r}-\mathbf{v}))\}_{\mathbf{v}\in\Gamma}$ provide useful approximations of the lowest two bands in the sense that

$$\varphi(\mathbf{r};\mathbf{k}) \approx \sum_{\mathbf{v}\in\Gamma} \left(\hat{A}(\mathbf{k})\phi_A(\mathbf{r}-\mathbf{v}) + \hat{B}(\mathbf{k})\phi_B(\mathbf{r}-\mathbf{v})\right) e^{i\mathbf{k}\cdot\mathbf{v}}. \tag{2.3}$$

Note that we omit the band index n because we are interested only in the lowest two bands. With this analytical construction of the Bloch modes, one can compute the dispersion relation. Furthermore, it turns out that the dispersion relation can be constructed from the coupled mode equation which describes the envelope dynamics.

In general, we note that a wave packet in $L^2(\mathbb{R}^2)$ associated with the lowest two bands can then be represented by

$$\psi(\mathbf{r}) \approx \sum_{\mathbf{p}\in\Gamma} \left(A_{\mathbf{p}}\phi_A(\mathbf{r}-\mathbf{p}) + B_{\mathbf{p}}\phi_B(\mathbf{r}-\mathbf{p})\right).$$

$\{(A_{\mathbf{p}}, B_{\mathbf{p}})\}_{\mathbf{p}\in\Gamma} \in l^2(\Gamma)$ is a natural representation of the continuous $L^2(\mathbb{R}^2)$ envelope associated with the lowest two bands. On the other hand, suppose that we are interested in the envelope dynamics; then $\{(A_{\mathbf{p}}(z), B_{\mathbf{p}}(z))\}_{\mathbf{p}\in\Gamma}$ satisfy the discrete coupled mode equation (2.4):

$$i\frac{dA_{\mathbf{p}}}{dz} + \mathcal{L}^- B_{\mathbf{p}} + \sigma|A_{\mathbf{p}}|^2 A_{\mathbf{p}} = 0, \tag{2.4a}$$

$$i\frac{dB_{\mathbf{p}}}{dz} + \mathcal{L}^+ A_{\mathbf{p}} + \sigma|B_{\mathbf{p}}|^2 B_{\mathbf{p}} = 0, \tag{2.4b}$$

where $z \in \mathbb{R}$ is the propagation distance, $\mathbf{p} \in \Gamma$, $\sigma = \pm 1$, and

$$\mathcal{L}^- B_{\mathbf{p}} = B_{\mathbf{p}} + \rho B_{\mathbf{p}-\mathbf{v}_1} + \rho B_{\mathbf{p}-\mathbf{v}_2},$$
$$\mathcal{L}^+ A_{\mathbf{p}} = A_{\mathbf{p}} + \rho A_{\mathbf{p}+\mathbf{v}_1} + \rho A_{\mathbf{p}+\mathbf{v}_2},$$

where $\rho > 0$ denote the ratio among the nearest neighbor hopping energies which can be different due to the deformation. For simplicity, we herein have assumed that two nearest neighbor hopping energies are the same and differ from the third one. The above system describes the dynamics of Bloch waves associated with the lowest two bands in a honeycomb lattice.

The discrete equation (2.4) has been shown to be a natural reduction of the above lattice NLS equation (2.1) in the strong potential limit: $|V| \gg 1$ [4, 2]. The discrete

system is easier to compute numerically and in turn leads to interesting continuous equations in the long wave limit. Detailed derivations and justifications can be found in [4, 2]. Many interesting physical problems can be directly described by this mode equation. Examples include the evolution of waves in Bose–Einstein condensates [16], conical and triangular diffraction in photonic crystals [4, 5], and exceptional point dynamics in $\mathcal{PT}$ symmetric lattices [28]. As indicated above, the discrete system (2.4) has been shown to replicate the phenomena of conical and triangular diffraction. Further, since the system is derived on an asymptotically slower timescale than the lattice NLS equation (2.1), computing with it is considerably faster.

Note that if a wave packet is associated with a specific wave number $\mathbf{k}$, then it can be conveniently represented by

$$\psi(\mathbf{r}) \approx \sum_{\mathbf{p}\in\Gamma} \left(a_{\mathbf{p}}\phi_A(\mathbf{r}-\mathbf{p}) + b_{\mathbf{p}}\phi_B(\mathbf{r}-\mathbf{p})\right) e^{i\mathbf{k}\cdot\mathbf{p}}.$$

For completeness we also give the equations of the discrete envelope in terms of the variables $\{(a_{\mathbf{p}}(z), b_{\mathbf{p}}(z))\}_{\mathbf{p}\in\Gamma}$ (see [4]):

$$i\frac{da_{\mathbf{p}}}{dz} + \mathcal{L}_{\mathbf{k}}^{-} b_{\mathbf{p}} + \sigma|a_{\mathbf{p}}|^2 a_{\mathbf{p}} = 0, \tag{2.5a}$$

$$i\frac{db_{\mathbf{p}}}{dz} + \mathcal{L}_{\mathbf{k}}^{+} a_{\mathbf{p}} + \sigma|b_{\mathbf{p}}|^2 b_{\mathbf{p}} = 0, \tag{2.5b}$$

where

$$\mathcal{L}_{\mathbf{k}}^{-} b_{\mathbf{p}} = b_{\mathbf{p}} + \rho b_{\mathbf{p}-\mathbf{v}_1} e^{-i\mathbf{k}\cdot\mathbf{v}_1} + \rho b_{\mathbf{p}-\mathbf{v}_2} e^{-i\mathbf{k}\cdot\mathbf{v}_2},$$
$$\mathcal{L}_{\mathbf{k}}^{+} a_{\mathbf{p}} = a_{\mathbf{p}} + \rho a_{\mathbf{p}+\mathbf{v}_1} e^{i\mathbf{k}\cdot\mathbf{v}_1} + \rho a_{\mathbf{p}+\mathbf{v}_2} e^{i\mathbf{k}\cdot\mathbf{v}_2}.$$

3. Linear dispersion relation of the discrete mode equation. The linear evolution equation (with constant coefficients) can be solved by using a discrete Fourier transform, i.e.,

$$\hat{A}(\mathbf{k}; z) = \sum_{\mathbf{v}\in\Gamma} A_{\mathbf{v}} e^{-i\mathbf{k}\cdot\mathbf{v}}$$

and

$$A_{\mathbf{v}} = \frac{1}{|\Omega'|}\int_{\Omega'} \hat{A}(\mathbf{k}) e^{i\mathbf{k}\cdot\mathbf{v}} d\mathbf{k},$$

where $|\Omega'|$ is the area of Ω'.

Substituting the Fourier mode $\left\{(\hat{A}(\mathbf{k}), \hat{B}(\mathbf{k}))e^{-i\mu z + i\mathbf{k}\cdot\mathbf{v}}\right\}_{\mathbf{v}\in\Gamma}$ into the linear discrete evolution problem associated with (2.4) leads to

$$\begin{pmatrix} \mu & \gamma(\mathbf{k}) \\ \gamma^*(\mathbf{k}) & \mu \end{pmatrix} \begin{pmatrix} \hat{A}(\mathbf{k}) \\ \hat{B}(\mathbf{k}) \end{pmatrix} = \begin{pmatrix} 0 \\ 0 \end{pmatrix}, \tag{3.1}$$

where $\gamma(\mathbf{k}) = 1 + \rho e^{-i\mathbf{k}\cdot\mathbf{v}_1} + \rho e^{-i\mathbf{k}\cdot\mathbf{v}_2}$ and the asterisk is used to denote the complex conjugate; i.e., $\gamma^*(\mathbf{k})$ is the complex conjugate of $\gamma(\mathbf{k})$. Note that, unlike the continuous Fourier transform, $\mathbf{k}$ takes only values in Ω' as opposed to all of $\mathbb{R}^2$. $\mu(\mathbf{k})$ is called the dispersion relation, which is defined only in the Brillouin zone Ω'; alternatively, $\mu(\mathbf{k})$ is continuous and periodic with two periods $\mathbf{k}_1$ and $\mathbf{k}_2$ in $\mathbb{R}^2$.

Here we choose the following characteristic vectors of the honeycomb lattice:

$$\mathbf{v}_1 = l\left(\frac{\sqrt{3}}{2}, \frac{1}{2}\right), \qquad \mathbf{v}_2 = l\left(\frac{\sqrt{3}}{2}, -\frac{1}{2}\right),$$
$$\mathbf{k}_1 = \frac{4\pi}{l\sqrt{3}}\left(\frac{1}{2}, \frac{\sqrt{3}}{2}\right), \qquad \mathbf{k}_2 = \frac{4\pi}{l\sqrt{3}}\left(\frac{1}{2}, -\frac{\sqrt{3}}{2}\right),$$

where l is the lattice constant.

Existence of nontrivial solutions of (3.1) requires that the determinant of the coefficient matrix be zero, which leads to the two branches of the dispersion relation

$$\mu_\pm(\mathbf{k}) = \pm\left|1 + \rho e^{-i\mathbf{k}\cdot\mathbf{v}_1} + \rho e^{-i\mathbf{k}\cdot\mathbf{v}_2}\right|. \tag{3.2}$$

We see that the dispersion relation has two branches: $\mu_+(\mathbf{k}) = -\mu_-(\mathbf{k})$. The two branches may or may not intersect with each other, depending on the value of ρ which measures the deformation. Let $\mathbf{K}_* = \mathbf{K}_*(\rho) \in \Omega'$ denote the special point(s) in the Brillouin zone such that $\mu_+(\mathbf{K}_*) = \min_{\mathbf{k}\in\Omega'}\mu_+(\mathbf{k})$ and $\mu_-(\mathbf{K}_*) = \max_{\mathbf{k}\in\Omega'}\mu_-(\mathbf{k})$. The values $(\mathbf{K}_*, \mu_\pm(\mathbf{K}_*))$ are band edges of the two branches. If the two branches intersect, $\mu_+(\mathbf{K}_*) = \mu_-(\mathbf{K}_*)$ and $(\mathbf{K}_*, \mu_\pm(\mathbf{K}_*))$ are the intersection points.

Using $\beta = 2\rho - 1$, a direct calculation shows the following:

1. If $\beta > 0$, then $\mathbf{K}_*$ has two values in the Brillouin zone Ω': $\mathbf{K}_* = \pm\mathbf{K} = \pm\frac{2}{l}\left(0, \pi - \arccos(\frac{1}{2\rho})\right)$ and $\mu_\pm(\mathbf{K}_*) = 0$. The two branches touch each other at these two points. The two points are called the Dirac points in the deformed honeycomb lattice. Near the $\mathbf{K}$ point, the dispersion relation has the leading expansion $\mu_\pm(\mathbf{K}+\mathbf{q}) = \pm\sqrt{q_1^2 + (\beta^2+2\beta)q_2^2} + o(|\mathbf{q}|)$, where $\mathbf{q} = (q_1, q_2)$ and $|\mathbf{q}| \ll 1$.
2. If $\beta = 0$, then $\mathbf{K}_*$ has only one value in the whole Brillouin zone Ω', $\mathbf{K}_* = \frac{1}{2}(-\mathbf{k}_1 - \mathbf{k}_2) = (\frac{4\pi}{l\sqrt{3}}, 0)$. In this critical case, the two Dirac points actually merge into one due to the underlying periodicity of $\mathbf{k} \in \mathbb{R}^2$. Namely, $\mathbf{K} \to \frac{2}{l}(0, \pi) = \frac{1}{2}(\mathbf{k}_1 - \mathbf{k}_2)$ as $\rho \to \frac{1}{2}$, and both $\frac{1}{2}(\mathbf{k}_1 - \mathbf{k}_2)$ and $-\frac{1}{2}(\mathbf{k}_1 - \mathbf{k}_2)$ are equivalent to $\frac{1}{2}(-\mathbf{k}_1 - \mathbf{k}_2) \in \Omega'$ due to the periodicity. Near the $\mathbf{K}_*$ point, the dispersion relation has the leading expansion $\mu_\pm(\mathbf{K}_* + \mathbf{q}) = \pm|q_1| + o(|\mathbf{q}|)$, where $\mathbf{q} = (q_1, q_2)$ and $|\mathbf{q}| \ll 1$.
3. If $\beta < 0$, then $\mathbf{K}_*$ has only one value in the whole Brillouin zone Ω', $\mathbf{K}_* = \frac{1}{2}(-\mathbf{k}_1 - \mathbf{k}_2) = (\frac{4\pi}{l\sqrt{3}}, 0)$. Note that $\mu_+(\mathbf{K}_*) > 0$ and $\mu_-(\mathbf{K}_*) < 0$, which means that the two dispersion branches separate from each other. In other words, there exists a gap between the two branches. Near $\mathbf{K}_*$ points, the dispersion relation has the leading expansion $\mu_\pm(\mathbf{K}_* + \mathbf{q}) = \pm\sqrt{\beta^2 + (1+\beta)^2 q_1^2} + o(|\mathbf{q}|)$, where $\mathbf{q} = (q_1, q_2)$ and $|\mathbf{q}| \ll 1$. It is seen that the width of the gap is $2|\beta|$.

Here we discuss only the regime where $0 < \rho \le 1$, i.e., $-1 < \beta \le 1$. Typical dispersion relations near $\mathbf{K}_*$ for different ρ values are illustrated in Figure 2.

4. Continuum limit and long wave approximation. In applications, the dynamics of the wide envelope associated with a specific value of $\mathbf{k}$ is of interest. For some situations, it is useful to derive a continuous system and analyze the continuous equation instead of the differential-difference equation; in this regard we derive continuous equations for our study of deformed lattices.

Suppose that the initial data of the discrete system is associated with a specific $\mathbf{k} \in \Omega'$ value, i.e.,

$$\{(A_\mathbf{p}, B_\mathbf{p})\,|_{z=0}\}_{\mathbf{p}\in\Gamma} = \{(a_\mathbf{p}, b_\mathbf{p})e^{i\mathbf{k}\cdot\mathbf{p}}\}_{\mathbf{p}\in\Gamma}.$$

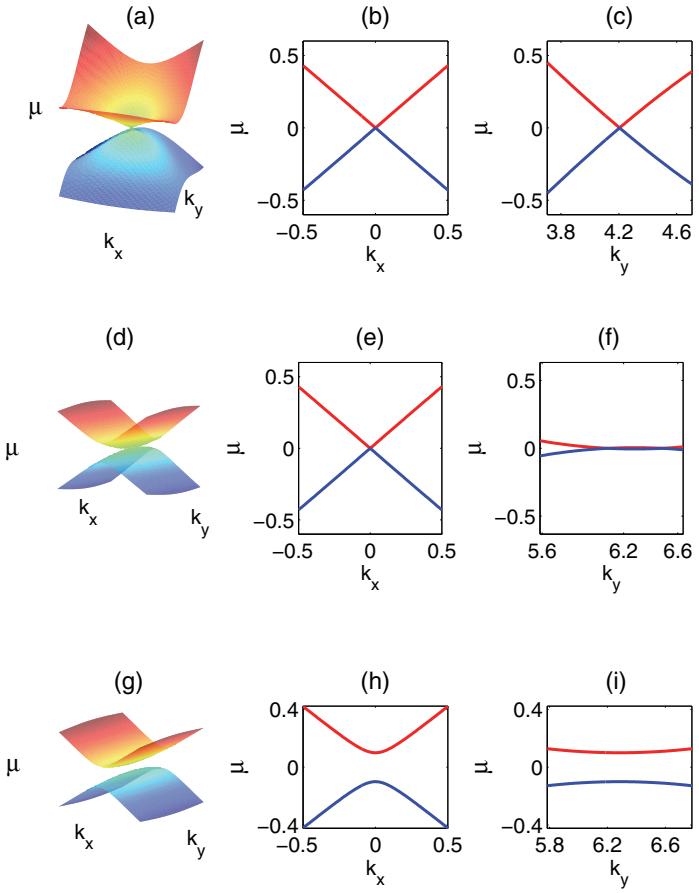

FIG. 2. *Typical dispersion relations.* (a)–(c) $\rho = 1$ *or* $\beta = 1$*;* (d)–(f) $\rho = 0.5025$ *or* $\beta = 0.005$*;* (g)–(i) $\rho = 0.45$ *or* $\beta = -0.1$. *The left figures are surface plots of the two branches near* $\mathbf{K}_*$*; the middle figures are the dispersion relations with fixed* $\mathbf{k}_y = \mathbf{K}_{*,y}$*; the right figures are the dispersion relations with fixed* $\mathbf{k}_x = \mathbf{K}_{*,x}$.

In addition, let us assume that the envelopes $\{(a_{\mathbf{v}}, b_{\mathbf{v}})\}_{\mathbf{p}\in\Gamma}$ change slowly in $\mathbf{p} \in \Gamma$. Namely, suppose that the envelope scale is much greater than the lattice scale. Then a long wave approximation can be employed; i.e., the characteristic length of the envelope δ is much greater than the lattice scale l.

The discrete envelope can be considered as the continuous envelope evaluated at the lattice points, i.e., $a_{\mathbf{p}}(z) = a(\mathbf{r} = \mathbf{p}, z)$ and $b_{\mathbf{p}}(z) = b(\mathbf{r} = \mathbf{p}, z)$; here the continuous transverse variable associated with the lattice is $\mathbf{r} = (r_1, r_2)$. In the long wave approximation, the continuous envelopes are assumed to depend only on the long wave envelope variables, and the amplitudes are small. Accordingly, we define $(a(\mathbf{r}, z), b(\mathbf{r}, z)) = \sqrt{\nu}(\tilde{a}(\mathbf{x}, \tilde{z}), \tilde{b}(\mathbf{x}, \tilde{z}))$, where the transverse variable is given by $\mathbf{x} = (x_1, x_2) = \mathbf{r}/\delta$ and the propagation variable by $\tilde{z} = \nu z$, where $\nu = \frac{\sqrt{3}\, l}{2\delta} \ll 1$, recalling that the lattice size is l.

Then the continuum limit and long wave approximation give that

$$\frac{da_{\mathbf{p}}(z)}{dz} = \sqrt{\nu}\nu\partial_{\tilde{z}}\tilde{a}(\mathbf{x},\tilde{z})$$

and

$$a_{\mathbf{p}+\mathbf{v}}(z) = \sqrt{\nu}\left(1 + \frac{1}{\delta}\sum_{m=1}^{2} v_m\partial_m + \frac{1}{2\delta^2}\sum_{m,n=1}^{2} v_m v_n \partial_{x_m,x_n} + \cdots\right)\tilde{a}(\mathbf{x},\tilde{z})\Big|_{\mathbf{x}=\mathbf{p}/\delta},$$

where $\mathbf{v} = (v_1, v_2)$, which is on the order of l. For convenience, we drop the tildes on top of $a(\mathbf{x},\tilde{z})$ and $b(\mathbf{x},\tilde{z})$ and replace $\tilde{z}$ by z in the following analysis.

Here we are interested only in the effective dynamics associated with the special point(s) $\mathbf{K}_*$. It turns out that if the initial envelope is associated with a value $\mathbf{k}$ which is far away from $\mathbf{K}_*$, then the continuous dynamics reduces to an effective NLS equation in a moving frame [4]. This is the case for most simple lattices. At $\mathbf{K} = \mathbf{K}_*$, as β changes from a positive number to a negative number, both the geometric structure of the dispersion relation and the associated effective wave dynamics change dramatically. We investigate different important cases next.

5. Effective envelope equations when two dispersion relation branches touch. In this regime, $\beta \geq 0$ and two branches touch each other at the Dirac point(s): $\mathbf{K}$ and $-\mathbf{K}$. Here we consider only the effective dynamics associated with $\mathbf{K}$; the analysis for $-\mathbf{K}$ is similar.

At $\mathbf{k} = \mathbf{K}$, $\mu_\pm = 0$ and by direct calculation we have

$$\rho e^{-i\mathbf{K}\cdot\mathbf{v}_1} + \rho e^{-i\mathbf{K}\cdot\mathbf{v}_2} = -1, \qquad \rho e^{-i\mathbf{K}\cdot\mathbf{v}_1} - \rho e^{-i\mathbf{K}\cdot\mathbf{v}_2} = -i\sqrt{4\rho^2 - 1}.$$

Let us define $\zeta = \sqrt{4\rho^2 - 1} = \sqrt{\beta^2 + 2\beta}$. Using Taylor expansion and evaluating at $\mathbf{k} = \mathbf{K}$, we have

$$\begin{aligned}\mathcal{L}_{\mathbf{K}}^{-} b_{\mathbf{p}} \sim \nu^{3/2}\Bigg[&\left(\partial_{x_1} + i\frac{\zeta}{\sqrt{3}}\partial_{x_2}\right) - \frac{\nu}{2}\left(\partial_{x_1}^2 + \frac{1}{3}\partial_{x_2}^2 + 2i\frac{\zeta}{\sqrt{3}}\partial_{x_1}\partial_{x_2}\right)\\ &+ \frac{\nu^2}{6}\left(\partial_{x_1}^3 + \frac{1}{3\sqrt{3}}\partial_{x_2}^3 + \partial_{x_1}\partial_{x_2}^2 + \sqrt{3}i\zeta\partial_{x_1}^2\partial_{x_2}\right)\Bigg] b + \cdots\end{aligned}$$

and

$$\begin{aligned}\mathcal{L}_{\mathbf{K}}^{+} a_{\mathbf{p}} \sim \nu^{3/2}\Bigg[&\left(-\partial_{x_1} + i\frac{\zeta}{\sqrt{3}}\partial_{x_2}\right) - \frac{\nu}{2}\left(\partial_{x_1}^2 + \frac{1}{3}\partial_{x_2}^2 - 2i\frac{\zeta}{\sqrt{3}}\partial_{x_1}\partial_{x_2}\right)\\ &- \frac{\nu^2}{6}\left(\partial_{x_1}^3 + \frac{1}{3\sqrt{3}}\partial_{x_2}^3 + \partial_{x_1}\partial_{x_2}^2 - \sqrt{3}i\zeta\partial_{x_1}^2\partial_{x_2}\right)\Bigg] a + \cdots.\end{aligned}$$

Introducing the variables $x = x_1$, $y = \frac{x_2}{\sqrt{3}}$ and keeping the Taylor expansion up to order ν^3, we have the following continuous equation:

$$i\partial_z a + (\partial_x + \mathcal{T}_1)b + \sigma|a|^2 a = 0, \tag{5.1a}$$

$$i\partial_z b + (-\partial_x + \mathcal{T}_2)a + \sigma|b|^2 b = 0, \tag{5.1b}$$

where

$$\begin{aligned}\mathcal{T}_1 &= i\zeta\partial_y - \frac{\nu}{2}\left(\partial_x^2 + \partial_y^2 + 2i\zeta\partial_x\partial_y\right) + \frac{\nu^2}{6}\left(\partial_x^3 + \partial_y^3 + 3\partial_x\partial_y^2 + 3i\zeta\partial_x^2\partial_y\right),\\ \mathcal{T}_2 &= i\zeta\partial_y - \frac{\nu}{2}\left(\partial_x^2 + \partial_y^2 - 2i\zeta\partial_x\partial_y\right) - \frac{\nu^2}{6}\left(\partial_x^3 + \partial_y^3 + 3\partial_x\partial_y^2 - 3i\zeta\partial_x^2\partial_y\right).\end{aligned}$$

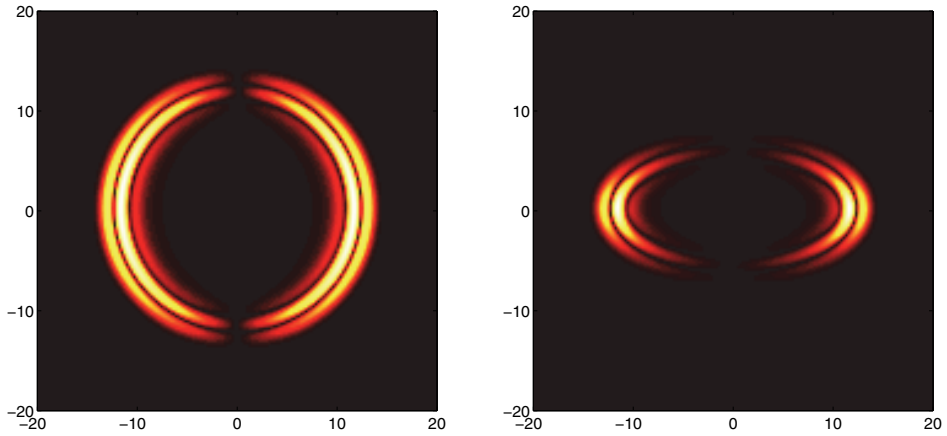

FIG. 3. *Conical and elliptical diffraction associated with the NLD equation* (5.2) *for* $\zeta = 1$ *(left) and* $\zeta = 0.5$ *(right) at* $z = 12$.

Note that $\mathcal{T}_2$ is the adjoint operator of $\mathcal{T}_1$ in $H^2(\mathbb{R}^2)$.

If $\beta = O(1)$, then $\zeta = O(1)$ and we have a maximally balanced leading order equation which is a nonlinear Dirac (NLD) equation:

$$i\partial_z a_0 + [\partial_x + i\zeta\partial_y]\, b_0 + \sigma|a_0|^2 a_0 = 0, \tag{5.2a}$$

$$i\partial_z b_0 + [-\partial_x + i\zeta\partial_y]\, a_0 + \sigma|b_0|^2 b_0 = 0, \tag{5.2b}$$

where $a = a_0 + a_1$, $b = b_0 + b_1$, and a_1, b_1 are on the order of ν. This is the leading order nontrivial envelope dynamics. The leading linear part is actually a two-dimensional wave equation which is a weakly dispersive system. Higher order effects can be studied by adding higher order dispersive terms to the above system. This system exhibits the so-called conical/elliptical diffraction phenomenon. Figure 3 shows that initial Gaussians evolve to expanding rings or ellipses with different values of ζ.

Next we consider $0 \le \beta \ll 1$, which we will use as one of the two small parameters, noting that $\zeta = \sqrt{\beta^2 + 2\beta} = O(\sqrt{\beta})$ (the other small parameter is ν). The leading order equation is a one-dimensional wave equation. The effective envelope dynamics is studied on an appropriate slower timescale. Accordingly, we introduce a slow timescale, $Z = \epsilon z$, where $\epsilon \ll 1$ will depend on ν and ζ to be defined later.

It is convenient to convert the coupled system (5.1) to a second order system. Namely,

$$\partial_z^2 a - \partial_x^2 a + (\partial_x(\mathcal{T}_2 - \mathcal{T}_1) + \mathcal{T}_1\mathcal{T}_2)a + \sigma\left[-i\partial_z(|a|^2 a) + (\partial_x + \mathcal{T}_1)(|b|^2 b)\right] = 0, \tag{5.3a}$$

$$\partial_z^2 b - \partial_x^2 b + (\partial_x(\mathcal{T}_2 - \mathcal{T}_1) + \mathcal{T}_2\mathcal{T}_1)b + \sigma\left[-i\partial_z(|b|^2 b) + (-\partial_x + \mathcal{T}_2)(|a|^2 a)\right] = 0, \tag{5.3b}$$

where we note that $\mathcal{T}_2\mathcal{T}_1 = \mathcal{T}_1\mathcal{T}_2$ in $H^2(\mathbb{R}^2)$.

We express a and b as

$$a = \sqrt{\epsilon}(a_0(z, x, y, Z) + a_1(z, x, y, Z)), \quad b = \sqrt{\epsilon}(b_0(z, x, y, Z) + b_1(z, x, y, Z)),$$

where a_0 and b_0 satisfy the leading order equations, and the dependence on z can be understood via the leading order equations while the dependence on Z will be given by the effective dynamics; a_1 and b_1 are remainders which are on the order of $O(\epsilon)$.

Define two moving frames, i.e., $\theta = x - z$ and $\eta = x + z$; hence a_0 and b_0 have the form

$$a_0 = F(\theta, y, Z) + G(\eta, y, Z),$$
$$b_0 = \tilde{F}(\theta, y, Z) + \tilde{G}(\eta, y, Z).$$

Furthermore, from the above equations we have

$$\partial_\theta(-iF + \tilde{F}) + \partial_\eta(iG + \tilde{G}) = 0$$

and

$$\partial_\theta(-i\tilde{F} - F) + \partial_\eta(i\tilde{G} - G) = 0.$$

Thus,

$$\partial_\theta(-iF + \tilde{F}) = 0$$

and

$$\partial_\eta(iG + \tilde{G}) = 0.$$

Hence to the leading order for decaying functions, $\tilde{F} = iF$ and $\tilde{G} = -iG$. We remark that the equation for the remainder a_1 is

$$\begin{aligned} 4\partial_\theta\partial_\eta a_1 = {} & h_1(a_0, b_0, a_1, b_1) + \mathcal{T}_{\theta,y}F + \mathcal{T}_{\eta,y}G + \epsilon\left(-2\partial_\theta\partial_Z F + 2\partial_\eta\partial_Z G\right) \\ & + \epsilon\sigma\left[2i\partial_\theta(|F|^2F + 2|G|^2F + G^2F^*) - 2i\partial_\eta(|G|^2G + 2|F|^2G + F^2G^*)\right], \end{aligned}$$

and the equation for the remainder b_1 is

$$\begin{aligned} 4\partial_\theta\partial_\eta b_1 = {} & h_2(a_0, b_0, a_1, b_1) + \mathcal{T}_{\theta,y}F + \mathcal{T}_{\eta,y}G + \epsilon\left(-2\partial_\theta\partial_Z F + 2\partial_\eta\partial_Z G\right) \\ & + \epsilon\sigma\left[2i\partial_\theta(|F|^2F + 2|G|^2F + G^2F^*) - 2i\partial_\eta(|G|^2G + 2|F|^2G + F^2G^*)\right], \end{aligned}$$

where the operator $\mathcal{T}_{\theta,y}$ is of the form

$$\mathcal{T}_{\theta,y} = -\zeta^2\partial_y^2 + i\zeta\nu(\partial_\theta^2\partial_y - \partial_y^3) - \frac{\nu^2}{12}\left(\partial_\theta^4 + 6\partial_\theta^2\partial_y^2 - 3\partial_y^4 + 4\partial_\theta\partial_y^3\right)$$

and $\mathcal{T}_{\eta,y}$ is exactly the same as $\mathcal{T}_{\theta,y}$ by changing θ to η. In order to ensure that the estimates of the remainder $a_1 = O(\epsilon)$, $b_1 = O(\epsilon)$ hold for large z, secular terms need to be removed. When we integrate a_1, secular terms arise from the pieces that are functions of θ or η alone, since the terms containing both θ and η are relatively higher order terms; all other higher order terms are in $h_j(a_0, b_0, a_1, b_1) = o(\epsilon + \nu^2 + \nu\zeta + \zeta^2)$, $j = 1, 2$. Removal of secular terms in the equation for b_1 leads to the same equations.

5.1. Effective envelope dynamics: Maximal balance I. In the regime $\beta = O(\nu^2)$ (i.e., $\nu^2 = O(\nu\zeta) = O(\zeta^2) = O(\beta)$) with $\epsilon = \nu^2 = O(\beta)$, removal of secular terms at order $O(\epsilon)$ leads to the following maximally balanced nonlinear equation for the right-moving component,

$$\partial_\theta\partial_Z F + \frac{1}{2}\mathcal{M}_1 F - \sigma i\partial_\theta(|F|^2F) = 0, \tag{5.4}$$

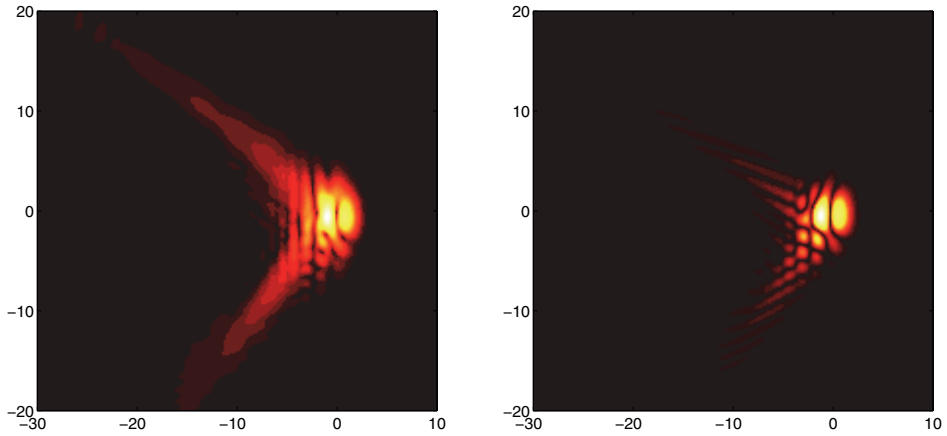

FIG. 4. *Left: Numerical simulation of the maximal balanced equation* (5.4). *Right: Numerical simulation of the NLSKP equation* (5.6). *In both simulations, the initial condition* $F(\theta, y, Z = 0) = \theta e^{-\theta^2 - y^2}$, $\sigma = +1$, *and* $\alpha_1 = 1$; *snapshot at* $Z = 1.2$. *The horizontal-vertical coordinate is* (θ, y).

and the left-moving component equation is

$$\partial_\eta \partial_Z G - \frac{1}{2}\mathcal{M}_1 G - \sigma i \partial_\eta (|G|^2 G) = 0,$$

where the operator $\mathcal{M}_1$ is defined as

$$\mathcal{M}_1 = \alpha_1^2 \partial_y^2 - i\alpha_1(\partial_\theta^2 \partial_y - \partial_y^3) + \frac{1}{12}\left(\partial_\theta^4 + 6\partial_\theta^2 \partial_y^2 - 3\partial_y^4 + 4\partial_\theta \partial_y^3\right)$$

and $\alpha_1 = \frac{\zeta}{\nu} = O(1)$. These two equations, (5.4) and (5.1), are nonlocal along the θ or η direction.

In this paper, we will not study the wave dynamics deeply in the reduced equations except in a few numerical simulations. The simulation given in Figure 4 shows the evolution given the initial data $F(\theta, y, Z = 0) = \theta e^{-\theta^2 - y^2}$, $\sigma = +1$. The original conical/elliptical diffraction when $\rho = 1$, $\rho = \frac{\sqrt{2}}{2}$ has now degenerated into nearly straight-line diffraction with some additional parabolic structure. The numerical schemes and related discussion on the initial conditions are discussed in section 7.

5.2. Effective envelope dynamics: Limit to the NLSKZ equation. In the regime $\beta \gg \nu^2$ (i.e., $\nu^2 \ll \nu\zeta \ll \zeta^2$) with $\epsilon = \zeta^2$, the removal of the secular terms at order $\mathcal{O}(\epsilon)$ leads to the two decoupled equations; the right-moving component is governed by

$$\partial_\theta \left(\partial_Z F - \sigma i |F|^2 F\right) + \frac{1}{2}\partial_y^2 F = 0, \tag{5.5}$$

and the left-moving component is governed by

$$\partial_\eta \left(\partial_Z G - \sigma i |G|^2 G\right) - \frac{1}{2}\partial_y^2 G = 0.$$

In fact, (5.5) results from the above maximal equation, (5.4), by taking $\alpha_1 \gg 1$ with the above choice of nonlinear scaling. In analogy with the results associated with the

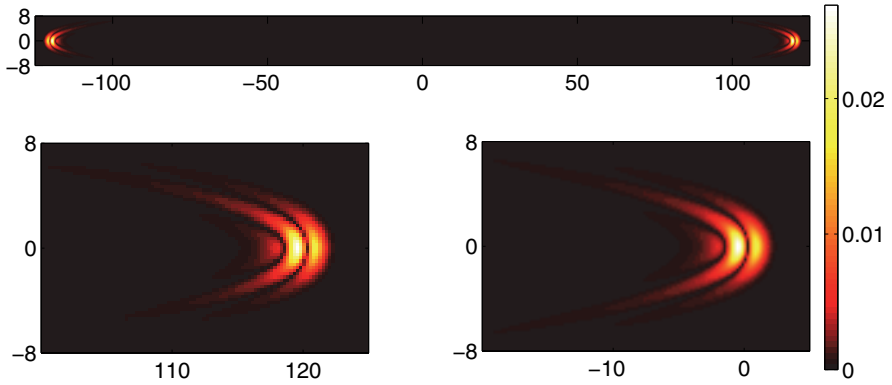

FIG. 5. *Numerical comparison between* (5.1) *and the NLSKZ equation,* (5.5). *Top: Intensity plot of the* $a(\mathbf{x}, z = 120)$ *with initial condition* $a(\mathbf{x}, 0) = b(\mathbf{x}, 0) = \sqrt{\epsilon} x e^{-x^2-y^2}$ *with* $\sigma = +1$ *and* $\zeta = 0.1$*; hence* $\epsilon = \zeta^2$ *in* (5.1). *Bottom left: Zoomed-in plot of the intensity of the right-moving component of the top figure, evaluated in the "fast" z coordinate at* $z = 120$. *Bottom right: Intensity plot of reduced equation* F *as evaluated at the "slow" time* $Z = 1.2$ *with initial data* $F(\theta, y, Z = 0) = \theta e^{-\theta^2-y^2}$, *where we recall that* $Z = \zeta^2 z = 10^{-2} z$, *or* $Z = 1.2$ *when* $z = 120$. *The horizontal-vertical coordinate for the top figure and bottom left figure is* (x, y)*; the horizontal-vertical coordinate for the bottom right figure is* (θ, y).

dispersionless KP equation, originally derived by Lin, Reissner, and Tsien [22], also known as the KZ equation [34], we call this the NLSKZ equation.

In Figure 5 the same initial condition as above is used: $F(\theta, y, Z = 0) = \theta e^{-\theta^2-y^2}$, $\sigma = +1$. We see a more distinctive parabolic shape than in Figure 4, obtained from the maximal balanced equation (5.4); both exhibit the straight-line diffraction pattern since the one-dimensional wave equation is the leading order equation. In this case we compare the results of (5.1) and (5.5). The intensity for F is scaled by a factor $\sqrt{\epsilon} = 0.1$.

5.3. Effective envelope dynamics: Near critical limit to the NLSKP equation. In the "near critical" regime when $\beta \ll \nu^2$ (i.e., $\zeta^2 \ll \nu^2$) we choose $\epsilon = \nu^2 \gg \beta$. Removal of secular terms leads to the decoupled equations; the right-moving component is governed by

$$\partial_\theta \left(\partial_Z F + \frac{1}{24} \left(\partial_\theta^3 + 6\partial_\theta \partial_y^2 + 4\partial_y^3 \right) F - \sigma i |F|^2 F \right) - \frac{1}{8} \partial_y^4 F = 0, \tag{5.6}$$

and the left-moving component is governed by

$$\partial_\eta \left(\partial_Z G - \frac{1}{24} \left(\partial_\eta^3 + 6\partial_\eta \partial_y^2 + 4\partial_y^3 \right) G - \sigma i |G|^2 G \right) + \frac{1}{8} \partial_y^4 G = 0.$$

In analogy with the results of the two-dimensional KP equation [19], we term the above equation an NLSKP-type equation, which can be obtained from the maximally balanced equation (5.4) by taking $\alpha_1 \ll 1$ with the above choice of nonlinear scaling. In Figure 4 we use the same initial conditions above, $F(\theta, y, Z = 0) = \theta e^{-\theta^2-y^2}$. We see that the pattern has properties similar to those above, but now we observe a tendency towards localization of the high intensity portion of the beam.

We recognize that (5.6) is not in complete analogy with how the KP equation modifies its one-dimensional counterpart Korteweg–de Vries equation [1]. A direct

NLS analogy would lead to the following form:

$$\partial_\theta \left(\partial_Z F + i\partial_\theta^2 F - \sigma i|F|^2 F\right) \pm \partial_y^2 F = 0. \tag{5.7}$$

Actually, (5.7) arises in a different deformation limit. We will study this in the future.

6. Two dispersion branches separate from each other: Spectral gap. When $-1 < \beta < 0$, $\min_{\mathbf{k}} \mu_+(\mathbf{k}) \gtrsim \max_{\mathbf{k}} \mu_-(\mathbf{k})$; i.e., there is a gap between two dispersion branches. The band edges to this gap for both branches are reached at $\mathbf{K}_* = -\frac{1}{2}\mathbf{k}_1 - \frac{1}{2}\mathbf{k}_2$. The width of the band gap is $2|\beta|$. It is convenient to introduce a new variable $\kappa = \frac{|\beta|}{\nu}$ so that the width of the gap is $2\kappa\nu$.

Taking the continuous limit from the discrete system (2.5), making use of the relation $\rho e^{-i\mathbf{K}_*\cdot\mathbf{v}_1} = \rho e^{-i\mathbf{K}_*\cdot\mathbf{v}_2} = -\rho$, keeping terms up to ν^2, and rescaling the variables $x = x_1, y = x_2/\sqrt{3}$, we obtain the continuous equations

$$i\partial_z a + (1-\kappa\nu)\mathcal{F}_1 b + \kappa b + \sigma|a|^2 a = 0, \tag{6.1a}$$

$$i\partial_z b + (1-\kappa\nu)\mathcal{F}_2 a + \kappa a + \sigma|b|^2 b = 0, \tag{6.1b}$$

where

$$\mathcal{F}_1 = \partial_x - \frac{\nu}{2}(\partial_x^2 + \partial_y^2) + \frac{\nu^2}{6}\left(\partial_x^3 + \partial_y^3 + 3\partial_x\partial_y^2\right),$$
$$\mathcal{F}_2 = -\partial_x - \frac{\nu}{2}(\partial_x^2 + \partial_y^2) - \frac{\nu^2}{6}\left(\partial_x^3 + \partial_y^3 + 3\partial_x\partial_y^2\right).$$

The operator $\mathcal{F}_2$ is the adjoint operator of $\mathcal{F}_1$ in $H^2(\mathbb{R}^2)$.

As before, we convert the above equations to a second order system which is of the form

$$\begin{aligned}
&\partial_z^2 a + \kappa^2 a + \kappa(1-\kappa\nu)(\mathcal{F}_1+\mathcal{F}_2)a + (1-\kappa\nu)^2\mathcal{F}_1\mathcal{F}_2 a \\
&\quad + \sigma\left[-i\partial_z(|a|^2 a) + (\kappa + (1-\kappa\nu)\mathcal{F}_1)(|b|^2 b)\right] = 0, \\
&\partial_z^2 b + \kappa^2 b + \kappa(1-\kappa\nu)(\mathcal{F}_1+\mathcal{F}_2)b + (1-\kappa\nu)^2\mathcal{F}_2\mathcal{F}_1 b \\
&\quad + \sigma\left[-i\partial_z(|b|^2 b) + (\kappa + (1-\kappa\nu)\mathcal{F}_2)(|a|^2 a)\right] = 0,
\end{aligned}$$

where the operator $\mathcal{F}_1\mathcal{F}_2$ reads

$$\mathcal{F}_1\mathcal{F}_2 = -\partial_x^2 - \frac{\nu^2}{12}\left(\partial_x^4 + 6\partial_x^2\partial_y^2 - 3\partial_y^4 + 4\partial_x\partial_y^3\right) + O(\nu^3).$$

We have two (generally small) parameters: ν and κ. Due to the different balances between these small parameters, we have different leading order equations.

In the regime where $|\beta| \ll \nu$, i.e., $\kappa \ll 1$, the dominant linear terms give rise to a wave equation. Similar to the above section, we introduce the moving coordinates $\theta = x - z$, $\eta = x + z$ and the slow scale $Z = \epsilon z$. Express a and b as

$$a = \sqrt{\epsilon}(a_0(\theta,\eta,y,Z) + a_1(\theta,\eta,y,Z)), \quad b = \sqrt{\epsilon}(b_0(\theta,\eta,y,Z) + b_1(\theta,\eta,y,Z)),$$

where a_0 and b_0 satisfy the leading order equations; a_1 and b_1 are remainders which are small and of order $O(\epsilon)$.

As above, a similar calculation shows that

$$a_0 = F(\theta,y,Z) + G(\eta,y,Z), \quad b_0 = iF(\theta,y,Z) - iG(\eta,y,Z).$$

We note that the equation for the remainder a_1 is

$$4\partial_\theta\partial_\eta a_1 = g_1(a_0,b_0,a_1,b_1) + \mathcal{F}_{\theta,y}F + \mathcal{F}_{\eta,y}G + \epsilon\left[-2\partial_\theta\partial_Z F + 2\partial_\eta\partial_Z G\right) + \epsilon\sigma\left[2i\partial_\theta(|F|^2F + 2|G|^2F + G^2F^*) - 2i\partial_\eta(|G|^2G + 2|F|^2G + F^2G^*)\right],$$

and the equation for the remainder b_1 is

$$4\partial_\theta\partial_\eta b_1 = g_2(a_0,b_0,a_1,b_1) + \mathcal{F}_{\theta,y}F + \mathcal{F}_{\eta,y}G + \epsilon\left(-2\partial_\theta\partial_Z F + 2\partial_\eta\partial_Z G\right) + \epsilon\sigma\left[2i\partial_\theta(|F|^2F + 2|G|^2F + G^2F^*) - 2i\partial_\eta(|G|^2G + 2|F|^2G + F^2G^*)\right],$$

where the operator $\mathcal{F}_{\theta,y}$ is of the form

$$\mathcal{F}_{\theta,y} = -\frac{\nu^2}{12}\left(\partial_\theta^4 + 6\partial_\theta^2\partial_y^2 - 3\partial_y^4 + 4\partial_\theta\partial_y^3\right) - \kappa\nu(\partial_\theta^2 + \partial_y^2) + \kappa^2$$

and $\mathcal{F}_{\eta,y}$ is obtained by changing θ to η; $g_j(a_0,a_1,b_0,b_1) = o(\epsilon+\kappa^2+\nu^2+\nu\kappa)$, $j = 1,2$, contain higher order terms.

6.1. Effective envelope dynamics: Maximal balance II. If $|\beta| = O(\nu^2)$, i.e., $\kappa = O(\nu)$, we choose $\epsilon = \nu^2$. All terms in $\mathcal{F}_{\theta,y}$ and $\mathcal{F}_{\eta,y}$ have the same order as ϵ. Removal of secular terms at order ϵ leads to two maximally balanced equations which govern the leading order dynamics of the right- and left-moving components; the equation for F is

$$\partial_\theta\partial_Z F + \frac{1}{2}\mathcal{M}_2 F - \sigma i\partial_\theta(|F|^2F) = 0, \tag{6.2}$$

and the equation for G is

$$\partial_\eta\partial_Z G - \frac{1}{2}\mathcal{M}_2 G + \sigma i\partial_\eta(|G|^2G) = 0,$$

where the operator $\mathcal{M}_2$ is defined as

$$\mathcal{M}_2 = -\alpha_2^2 + \alpha_2(\partial_\theta^2 + \partial_y^2) + \frac{1}{12}\left(\partial_\theta^4 + 6\partial_\theta^2\partial_y^2 - 3\partial_y^4 + 4\partial_\theta\partial_y^3\right)$$

and $\alpha_2 = \frac{|\beta|}{\nu^2}$.

The evolution pattern of this equation, (6.2), is exhibited in Figure 6. It is similar to the NLSKP case (see Figure 4), but this pattern has additional transverse dispersion.

6.2. Effective envelope dynamics: Near critical limit from the gap regime to NLSKP. If $\alpha_2 \ll 1$ or $|\beta| \ll \nu^2$ (i.e., $\kappa \ll \nu$), then a limiting form of the maximal balanced equation (6.2) with $\epsilon = \nu^2$ leads to two decoupled NLSKP equations; the right-moving component is governed by

$$\partial_\theta\left(\partial_Z F + \frac{1}{24}\left(\partial_\theta^3 + 6\partial_\theta\partial_y^2 + 4\partial_y^3\right)F - \sigma i|F|^2F\right) - \frac{1}{8}\partial_y^4 F = 0, \tag{6.3}$$

and the equation for the left moving component is of the form

$$\partial_\eta\left(\partial_Z G - \frac{1}{24}\left(\partial_\eta^3 + 6\partial_\eta\partial_y^2 + 4\partial_y^3\right) - \sigma i|G|^2G\right) + \frac{1}{8}\partial_y^4 G = 0.$$

This is essentially the same as what we have derived in subsection 5.3. Since this equation was numerically considered earlier, there is no reason to carry out further numerical calculations here.

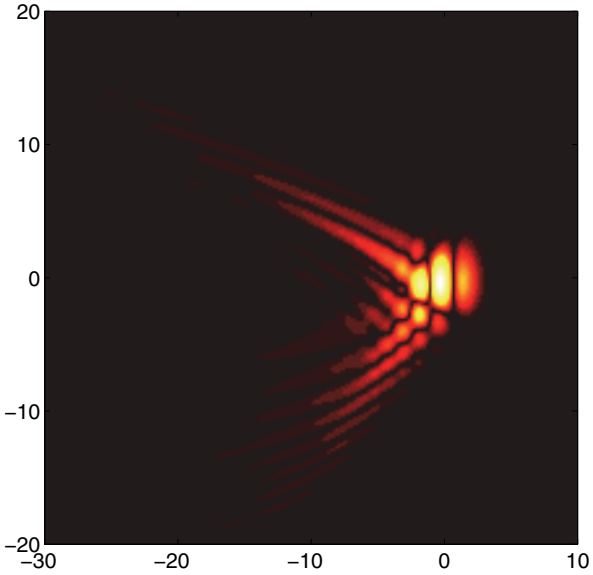

FIG. 6. *Numerical simulation of the maximally balanced equation* (6.2) *with* $F(\theta, y, Z = 0) = \theta e^{-\theta^2 - y^2}$ *and* $\alpha_2 = 1$. *Note the similarity to the near critical case of NLSKP (see Figure* 4*), but this case has additional transverse dispersion. The horizontal-vertical coordinate is* (θ, y).

6.3. Effective envelope dynamics: Limit to a nonlocal 1+1-dimensional evolution equation. When $\alpha_2 \gg 1$ with $\nu^2 \ll |\beta| \ll \nu$ (i.e, $\nu \ll \kappa \ll 1$), the limit of (6.2) with $\epsilon = \kappa^2$ leads to two decoupled 1+1-dimensional nonlinear evolution equations; the right-moving component is

$$\partial_\theta \left(\partial_Z F - \sigma i |F|^2 F\right) - \frac{1}{2} F = 0, \tag{6.4}$$

and the left-moving component is

$$\partial_\eta \left(\partial_Z G - \sigma i |G|^2 G\right) + \frac{1}{2} G = 0.$$

This is a nonlocal cubic self-phase equation (NCSP). Notice that there are no transverse dispersive terms in the above decoupled equations; they are nonlocal 1+1-dimensional modifications of the NLS equation. Thus in analogy with the region near $\rho = 1/2$ with Dirac points, in the gap region near $\rho = 1/2$ we see that there is a maximally balanced equation, (6.2), from which the other two equations, (6.3) and (6.4), result as limiting cases.

In Figure 7 for the same initial conditions as chosen earlier, we compare the high order continuous equation, (6.1), and the reduced 1+1-dimensional equation, (6.4). We see that they agree well and that there is a stronger tendency towards localization of the beam, whereas in Figure 6 there was significant transverse variation.

6.4. Effective envelope dynamics: NLD equation with nonzero mass. Next we turn to the gap region where the gap width is larger than in the previous cases; in particular we next consider $|\beta| = O(\nu)$. In this regime, the leading order equation is no longer the 1+1-dimensional nondispersive wave equation. Neglecting

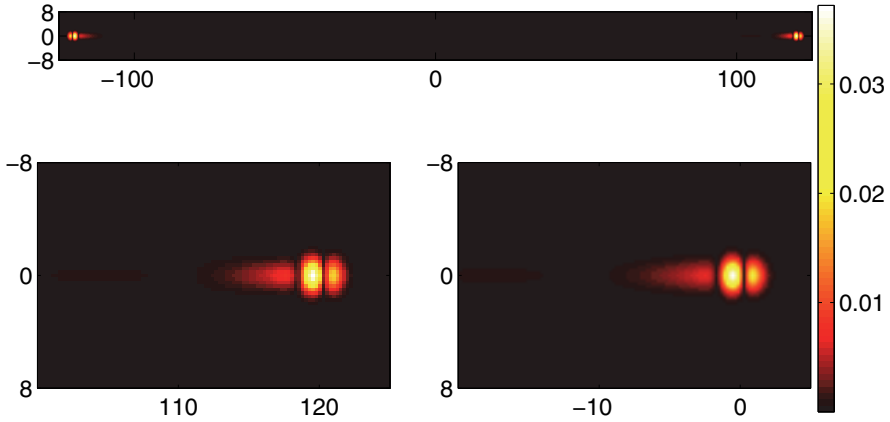

FIG. 7. *Numerical comparison between equations* (6.1) *and* (6.4). *Top: Intensity plot of the* $a(\mathbf{x}, z = 120)$ *with initial condition* $a(\mathbf{x}, 0) = b(\mathbf{x}, 0) = \sqrt{\epsilon} x e^{-x^2-y^2}$ *with* $\sigma = +1$ *and* $\beta = -0.001$, $\nu = 0.01$ *in* (5.1). *Bottom left: Zoomed-in plot of the intensity of the right-moving component. Bottom right: Intensity plot of* $F(\theta, y, Z = 1.2)$*; note that* $\nu \ll \kappa \ll 1$. *Also recall that* $Z = \epsilon z$, *where* $\kappa = 0.1, \epsilon = \kappa^2 = 10^{-2}$. *The horizontal-vertical coordinate for the top figure and bottom left figure is* $x - y$*; the horizontal-vertical coordinate for the bottom right figure is* $\theta - y$.

higher order terms in the coupled system (6.1), we have a leading order equation of the form

$$i\partial_z a_0 + \partial_x b_0 + \kappa b_0 + \sigma |a_0|^2 a_0 = 0, \tag{6.5a}$$

$$i\partial_z b_0 - \partial_x a_0 + \kappa a_0 + \sigma |b_0|^2 b_0 = 0. \tag{6.5b}$$

Note that $\kappa = \frac{|\beta|}{\nu} = O(1)$ in this regime. This is a one-dimensional nonlinear Dirac equation with nonzero mass (NLDM). Interestingly it admits localized soliton solutions and kink solutions [11]. This is consistent with the expectation that in regions where there is a gap in the spectrum, localized solutions can occur.

6.5. Effective envelope dynamics: NLS equation. In the regime $\nu \ll |\beta| \ll 1$ (i.e., $\nu \ll \kappa^{-1} \ll 1$), which has an asymptotically larger spectral gap width than the prior regime, the leading order equation yields a phase modulation, i.e.,

$$\partial_z^2 a_0 + \kappa^2 a_0 = 0, \quad \partial_z^2 b_0 + \kappa^2 b_0 = 0.$$

It is useful to introduce the variables $\bar{z} = \kappa z$ and $Z = \epsilon \bar{z}$ and express a and b as

$$a = \sqrt{\epsilon\kappa}(a_0(\bar{z}, Z, x, y) + a_1(\bar{z}, Z, x, y)), \quad b = \sqrt{\epsilon\kappa}(b_0(\bar{z}, Z, x, y) + b_1(\bar{z}, Z, x, y)),$$

where a_0 and b_0 satisfy the leading order equations; a_1 and b_1 are remainders which are small.

We have the following solutions for a_0 and b_0:

$$a_0 = P(Z, x, y)e^{i\bar{z}} + Q(Z, x, y)e^{-i\bar{z}},$$
$$b_0 = P(Z, x, y)e^{i\bar{z}} - Q(Z, x, y)e^{-i\bar{z}}.$$

Substituting the expansion into the equation for a, we obtain the equation for a_1

as

$$
\begin{aligned}
-(\partial_{\bar z}^2 a_1 + a_1) = {} & f_1(a_0, b_0, a_1, b_1) + 4\epsilon\sigma Q^2 \bar P e^{-3i\bar z} - 2\epsilon P^2 \bar Q e^{3i\bar z} \\
& + e^{i\bar z}\left(\epsilon 2i\partial_Z P - \kappa^{-1}\nu(\partial_x^2 + \partial_y^2)P - \kappa^{-2}\partial_x^2 P + 2\epsilon\sigma(|P|^2 + 2|Q|^2)P\right) \\
& + e^{-i\bar z}\left(-\epsilon 2i\partial_Z Q - \kappa^{-1}\nu(\partial_x^2 + \partial_y^2)Q - \kappa^{-2}\partial_x^2 P - 2\epsilon\sigma(|Q|^2 + 2|P|^2)Q\right),
\end{aligned}
$$

and the equation for b_1 is

$$
\begin{aligned}
-(\partial_{\bar z}^2 b_1 + b_1) = {} & f_2(a_0, b_0, a_1, b_1) + 4\epsilon\sigma Q^2 \bar P e^{-3i\bar z} - 2\epsilon P^2 \bar Q e^{3i\bar z} \\
& + e^{i\bar z}\left(\epsilon 2i\partial_Z P - \kappa^{-1}\nu(\partial_x^2 + \partial_y^2)P - \kappa^{-2}\partial_x^2 P + 2\epsilon\sigma(|P|^2 + 2|Q|^2)P\right) \\
& + e^{-i\bar z}\left(-\epsilon 2i\partial_Z Q - \kappa^{-1}\nu(\partial_x^2 + \partial_y^2)Q - \kappa^{-2}\partial_x^2 P - 2\epsilon\sigma(|Q|^2 + 2|P|^2)Q\right),
\end{aligned}
$$

where $f_i(a_0, b_0, a_1, b_1) = o(\epsilon, \kappa^{-2}, \nu\kappa^{-1})$ contain all higher order terms.

Removal of secular terms leads at order ϵ (note that $\epsilon = \kappa^{-2} = \frac{\nu^2}{\beta^2}$) to the following one-dimensional focusing-defocusing NLS equations:

$$
i\partial_Z P - \frac{1}{2}\partial_x^2 P + \sigma(|P|^2 + 2|Q|^2)P = 0, \tag{6.6a}
$$

$$
i\partial_Z Q + \frac{1}{2}\partial_x^2 Q + \sigma(|Q|^2 + 2|P|^2)Q = 0, \tag{6.6b}
$$

where the dispersion along the y direction contained in the terms $(\partial_x^2 + \partial_y^2)P$ and $(\partial_x^2 + \partial_y^2)Q$ is of smaller order and hence omitted in the leading order dominant equation. It should be noted that when $|\beta|$ becomes larger, the dispersive terms along the y direction become stronger. We also note that if, say, $P = 0$ initially, it remains zero, and then standard NLS equations result for Q; this equation admits localized soliton solutions if $\sigma = +1$. We also see that NLS gap solitons can exist only when the gap is wide enough compared to the envelope, i.e., $|\beta| \gg \nu$. A similar discussion can be used to establish that if $|\beta| = O(1)$, the governing equation would be a two-dimensional NLS equation. Interested readers can refer to [4].

7. Summary: Asymptotic equations due to deformations. Here we refer to Figure 8, which conveniently illustrates the regimes where the reduced equations are located in a (ν, β) diagram.

We see that in the regime where β and ν are small there are two parabolic regions $|\beta| = \pm\nu^2$ in which maximal balanced equations arise. These and other limiting equations as well as their regions of validity are given in the figure.

In this paper we have used numerical simulations to exhibit the dynamics corresponding to the different regimes and to elucidate our analysis. The numerical scheme that we used is the spectral method equipped with an ETDRK4 method [20]. We simulated all the nonlocal-type equations and chose typical examples to compare the dynamics between the original multiscale long wave envelope equations and corresponding reduced effective envelope equations. The results are shown in the respective sections in which the equations are derived.

Based on the behavior of the KP equation [1], the initial condition is required to satisfy the constraint

$$
\int_{\mathbb{R}} F(\theta, y, Z)\, d\theta = 0. \tag{7.1}
$$

In [3], this constraint is discussed in more detail, as well as its effect on the decay and regularity of solutions. The decay and regularity of solutions associated with

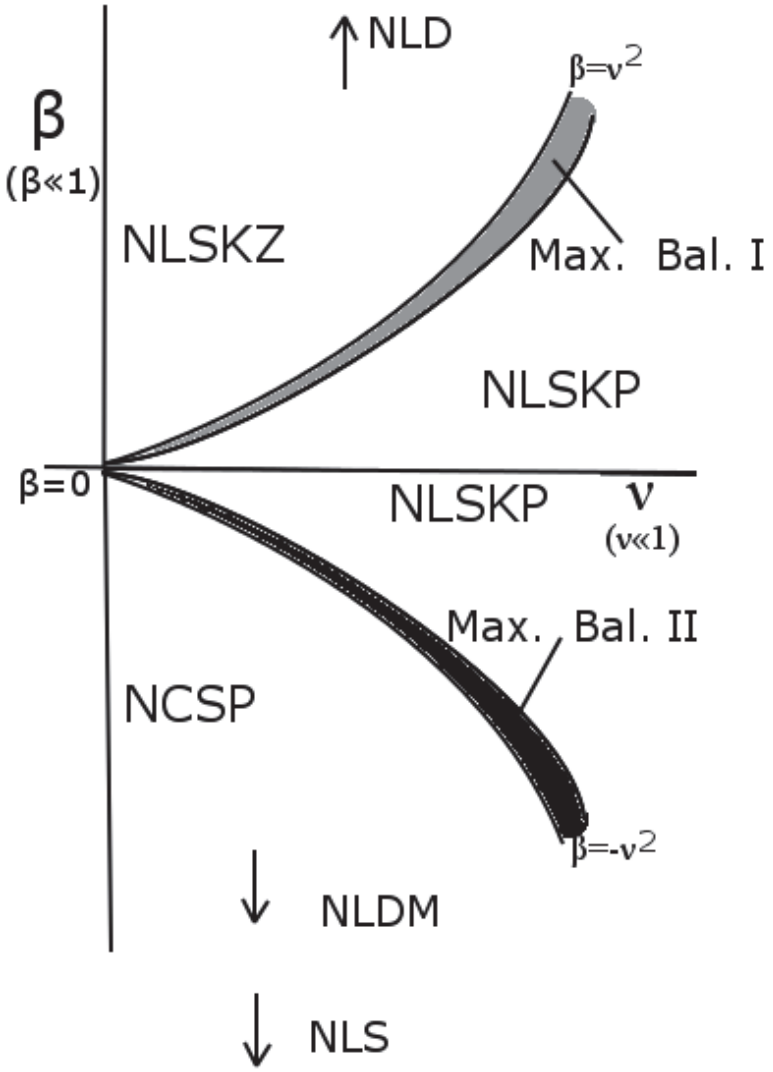

FIG. 8. *This schematic figure shows the various regimes where the reduced asymptotic equations are located in the* (ν, β) *plane. Two maximal balanced equations,* (5.4) *and* (6.2)*, arise in the two parabolic regions* $|\beta| = O(\nu^2)$*. When* $|\beta| \ll \nu^2$*, the NLSKP equations,* (5.6)*, are dominant. When* $\nu^2 \ll \beta \ll 1$*, two dispersionless equation, NLSKZ* (5.5) *and NCSP* (6.4)*, arise. When* $\nu^2 \ll |\beta| \ll \nu$*, the massless NLD* (5.2) *and the NLDM* (6.5) *are obtained. When* $\nu \ll |\beta| \ll 1$*, a* $2+1$ *NLD* (5.2) *and NLS-type equations are obtained.*

the equations derived here remain for future investigation. We choose the initial conditions $F(\theta, y, Z = 0) = \theta e^{-\theta^2 - y^2}$ for the reduced equations. This initial data satisfies the constraint (7.1). Accordingly, in (5.1) and (6.1) we choose $a(\mathbf{x}, z = 0) = b(\mathbf{x}, z = 0) = \sqrt{\epsilon} x e^{-x^2 - y^2}$, where the values of ϵ are chosen to be consistent with the parameter regimes governing the reduced equations.

8. Conclusion and discussion. This work studies the effective or reduced asymptotic dynamics of Bloch waves in deformed honeycomb lattices. In honey-

comb lattices the lowest two bands of the dispersion relation of the lattice can touch each other at isolated points, termed Dirac points. The corresponding Bloch wave dynamics associated are governed by nonlinear discrete Dirac equations—see (2.4) or (2.5). However, as discussed here, the location of the Dirac points may change and even disappear when the lattices are deformed. This work gives a comprehensive description of the essential dynamics associated with the deformation process. The goal of this study is to derive the effective long wave ($\nu \ll 1$) envelope equations in the interesting parameter deformation regimes, $-1 < \beta < 1$, $0 < \rho < 1$, and $\beta = 2\rho - 1$, and develop some basic understanding of the phenomena these equations describe. The well-posedness of the reduced equations and rigorous asymptotic estimates are interesting questions but are outside the scope of this work.

In the regions sufficiently close to the merging of Dirac points and appearance of a small gap in the spectrum ($|\beta| = O(\nu^2)$) there are two main equations, depending on whether there are Dirac points ($\beta > 0$) or there is a gap ($\beta < 0$) in the spectrum between the two dispersion branches. When there are Dirac points, the main equation is (5.4); on the other hand, when there is a sufficiently small gap, the main equation is (6.2).

The main equation (5.4) has two limits: an NLSKZ equation (5.5) when $\beta \gg \nu^2$, and an NLSKP-type equation (5.6) when we are extremely close to the merging point, $\beta \ll \nu^2$. The equations (5.4)–(5.6) also show how conical and elliptical diffraction modify into straight-line diffraction.

When we are close to $\beta = 0$ but the Dirac points disappear and there is a gap in the spectrum, the main equation (6.2) limits to cases when the gap is very narrow, in which case the governing equation is still an NLSKP-type equation—see (5.6). At larger values of the gap width, the main equation (6.2) limits to a modified nonlocal 1+1-dimensional modification of the NLS equation; see (6.4).

When the gap width is comparable to the envelope scale, the governing equation becomes a Dirac equation with nonzero mass, (6.5). When the gap width is even larger, the governing equation is then a coupled focusing-defocusing NLS equation, (6.6). Both the NLDM and NLS equations indicate the existence of gap solitons.

Finally, it is remarkable that there are many asymptotically interesting equations that result from the discrete systems (2.4) or equivalently (2.5). This is a reflection of the fact that these discrete equations are derived from an underlying physically very important equation: the lattice NLS equation (2.1) with a honeycomb potential.

Acknowledgments. The authors are grateful to Professor William L. Kath and to the referees for useful comments and suggestions.

REFERENCES

[1] M. Ablowitz and H. Segur, *On the evolution of packets of water waves*, J. Fluid Mech., 92 (1979), pp. 691–715.

[2] M. J. Ablowitz, C. W. Curtis, and Y. Zhu, *On tight-binding approximations in optical lattices*, Stud. Appl. Math., 129 (2013), pp. 362–388.

[3] M. J. Ablowitz and J. Villarroel, *On the Kadomtsev-Petviashili equation and associated constraints*, Stud. Appl. Math., 85 (1991), pp. 195–213.

[4] M. J. Ablowitz and Y. Zhu, *Evolution of Bloch-mode envelopes in two-dimensional generalized honeycomb lattices*, Phys. Rev. A, 82 (2010), 013840.

[5] M. J. Ablowitz and Y. Zhu, *Unified orbital description of the envelope dynamics in two-dimensional simple periodic lattices*, Stud. Appl. Math., 131 (2013), pp. 41–71.

[6] M. J. Ablowitz and Y. Zhu, *Nonlinear waves in shallow honeycomb lattices*, SIAM J. Appl. Math., 72 (2012), pp. 240–260.

[7] D. Agueev and D. Pelinovsky, *Modeling of wave resonances in low-contrast photonic crystals*, SIAM J. Appl. Math., 65 (2005), pp. 1101–1129.
[8] O. Bahat-Treidel, O. Peleg, M. Grobman, N. Shapira, M. Segev, and T. Pereg-Barnea, *Klein tunneling in deformed honeycomb lattices*, Phys. Rev. Lett., 104 (2010), 063901.
[9] O. Bahat-Treidel, O. Peleg, and M. Segev, *Symmetry breaking in honeycomb photonic lattices*, Opt. Lett., 33 (2008), pp. 2251–2253.
[10] O. Bahat-Treidel, O. Peleg, M. Segev, and H. Buljan, *Breakdown of Dirac dynamics in honeycomb lattices due to nonlinear interactions*, Phys. Rev. A, 82 (2010), 013830.
[11] M. Conforti, C. De Angelis, and T. R. Akylas, *Energy localization and transport in binary waveguide arrays*, Phys. Rev. A, 83 (2011), 043822.
[12] T. Dohnal and A. B. Aceves, *Optical soliton bullets in $(2+1)$D nonlinear Bragg resonant periodic geometries*, Stud. Appl. Math., 115 (2005), pp. 209–232.
[13] C. L. Fefferman and M. Weinstein, *Honeycomb lattice potentials and Dirac points*, J. Amer. Math. Soc., 25 (2012), pp. 1169–1220.
[14] C. L. Fefferman and M. Weinstein, *Wave packets in honeycomb structures and two-dimensional Dirac equations*, Comm. Math. Phys., to appear; preprint available at arXiv:1212.6072.
[15] R. H. Goodman, M. I. Weinstein, and P. J. Holmes, *Nonlinear propagation of light in one-dimensional periodic structures*, J. Nonlinear Sci., 11 (2001), pp. 123–168.
[16] L. H. Haddad and L. C. Carr, *The nonlinear Dirac equation in Bose-Einstein condensates: Foundation and symmetries*, Phys. D, 238 (2009), pp. 1413–1421.
[17] F. D. M. Haldane and S. Raghu, *Possible realization of directional optical waveguides in photonic crystals with broken time-reversal symmetry*, Phys. Rev. Lett., 100 (2008), 013904.
[18] B. Ilan and M. I. Weinstein, *Band-edge solitons, nonlinear Schrödinger/Gross–Pitaevskii equations and effective media*, Multiscale Model. Simul., 8 (2010), pp. 1055–1101.
[19] B. B. Kadomtsev and V. Petviashvili, *On the stability of solitary waves in weakly dispersive media*, Sov. Phys. Dokl., 15 (1970), pp. 539–541.
[20] A.-K. Kassam and L. N. Trefethen, *Fourth-order time-stepping for stiff PDEs*, SIAM J. Sci. Comput., 26 (2005), pp. 1214–1233.
[21] P. G. Kevrekidis, B. A. Malomed, and Y. B. Gaididei, *Solitons in triangular and honeycomb dynamical lattices with the cubic nonlinearity*, Phys. Rev. E, 66 (2002), 016609.
[22] C. C. Lin, E. Reissner, and H. S. Tsien, *On two dimensional non steady motion of a slender body in a compressible fluid*, J. Math. Phys., 27 (1948), pp. 220–231.
[23] O. Morsch and M. Oberthaler, *Dynamics of Bose-Einstein condensates in optical lattices*, Rev. Modern Phys., 1 (2006), pp. 179–215.
[24] K. S. Novoselov, A. K. Geim, S. V. Morozov, D. Jiang, M. I. Katsnelson, I. V. Grigorieva, S. V. Dubonos, and A. A. Firsov, *Two-dimensional gas of massless Dirac fermions in graphene*, Nature, 438 (2005), pp. 197–200.
[25] K. S. Novoselov, A. K. Geim, S. V. Morozov, D. Jiang, Y. Zhang, S. V. Dubonos, I. V. Grigorieva, and A. A. Firsov, *Electric field effect in atomically thin carbon films*, Science, 306 (2004), pp. 666–669.
[26] O. Peleg, G. Bartal, B. Freedman, O. Manela, M. Segev, and D. N. Christodoulides, *Conical diffraction and gap solitons in honeycomb photonic lattices*, Phys. Rev. Lett., 98 (2007), 103901.
[27] C. J. Pethick and H. Smith, *Bose-Einstein Condensation in Dilute Gases*, Cambridge University Press, New York, 2001.
[28] H. Ramezani, T. Kottos, V. Kovanis, and D. N. Christodoulides, *Exceptional-point dynamics in photonic honeycomb lattices with $\mathcal{PT}$ symmetry*, Phys. Rev. A, 85 (2012), 013818.
[29] M. Reed and B. Simon, *Methods of Mathematical Physics* IV: *Analysis of Operators*, Academic Press, New York, 1978.
[30] Z. Shi and J. Yang, *Solitary waves bifurcated from Bloch-band edges in two-dimensional periodic media*, Phys. Rev. E, 75 (2007), 056602.
[31] C. Sparber, *Effective mass theorems for nonlinear Schrödinger equations*, SIAM J. Appl. Math., 66 (2006), pp. 820–842.
[32] C. Sulem and P. L. Sulem, *The Nonlinear Schrödinger Equation: Self-Focusing and Wave Collapse*, Springer, Berlin, 1999.
[33] J. Yang, *Nonlinear Waves in Integrable and Nonintegrable Systems*, Math. Model. Comput. 16, SIAM, Philadelphia, 2010.
[34] E. A. Zabolots and R. V. Khokhlov, *Quasi-plane waves in the nonlinear acoustics of confined beam*, Sov. Phys. Acous., 15 (1969), pp. 35–40.
[35] S. L. Zhu, B. Wang, and L. M. Duan, *Simulation and detection of Dirac fermions with cold atoms in an optical lattice*, Phys. Rev. Lett., 98 (2007), 260402.